Theoretical and numerical method in aeroacoustics

Maria ALEXANDRESCU, Nicuşor ALEXANDRESCU

INCAS - National Institute for Aerospace Research "Elie Carafoli"
Bdul Iuliu Maniu 220, Bucharest 061136, Romania
malex@incas.ro

DOI: 10.13111/2066-8201.2010.2.2.1

Abstract: *The paper deals with the mathematical and numerical modeling of the aerodynamic noise generated by the fluid flow interaction with the solid structure of a rotor blade.*
Our analysis use Lighthill's acoustic analogy. Lighthill idea was to express the fundamental equations of motion into a wave equation for acoustic fluctuation with a source term on the right-hand side. The obtained wave equation is solved numerically by the spatial discretization. The method is applied in the case of monopole source placed in different points of blade surfaces to find this effect of noise propagation.

Key Words: noise, aero-acoustic, discretization

1. INTRODUCTION

The sound (noise) can be regarded as a pressure disturbance which propagates through a fluid at acoustic velocity. The disturbances are usually associated with fluctuations overlapping the atmospheric pressure and are emitted by certain sources.

The sound sources are generated by motion, either by the free fluid motion, either by a solid body-fluid interaction. Additionally, heat sources may lead to noise generation. Sound sources can also be generated by the fluid flow interaction with a solid structure (such as a propeller). In this case, acoustic sources, beside those due to the turbulence, arise from the motion of the blades. Fig.1 presents possible sources of noise for the outer part of a rotor blade, surrounded by a fluid flow.

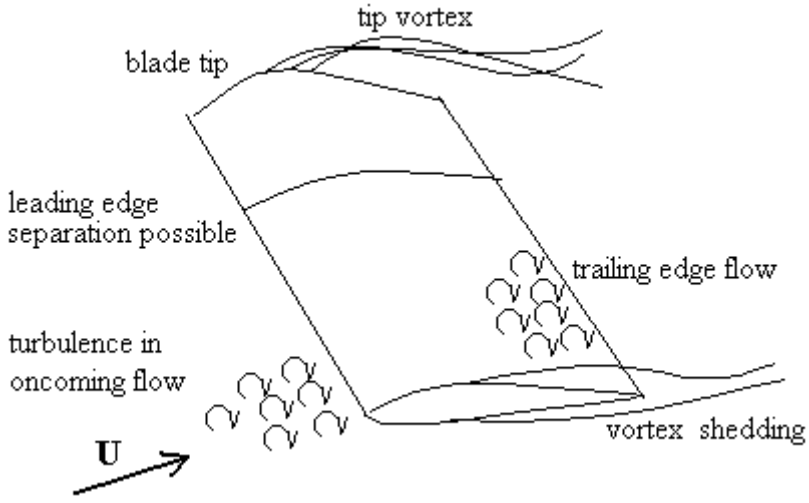

Fig.1. Sources of noise, flow around the outer part of the rotor blade

One can have the turbulent flow approaching the leading edge of the blade. The boundary layer that develops initially along the blade can be laminar. However, the transition from laminar to turbulent is expected due to the high Reynolds number flow. Close to the leading edge on the upper side of the blade, the flow accelerates first. Further downstream the flow decelerates again. Boundary-layer separation may occur due to sufficiently large adverse pressure gradient, which decelerates the fluid close to the solid surface to rest. A separation point will appear and the boundary layer detaches from the surface. Behind the trailing edge, due to the differences in the velocity streams (pressures) with the vorticity shed from the blade. At the tip of the blade the pressure difference between the suction and pressure side forms the tip vortex. All these phenomena contribute to noise generation.

2. LIGHTHILL'S ACOUSTIC ANALOGY [1]

Lighthill's acoustic analogy was the first attempt to describe the radiation of the sound generated by a turbulent flow. The analogy is based on the hypothesis that the part of the flow field which is the source for acoustics is distinct, so that the acoustic wave does not interfere with the flow. The governing equations for a compressible fluid motion are the conservation laws of mass, momentum and energy:

$$\frac{\partial \rho}{\partial t} + \frac{\partial}{\partial x_i}\left(\rho u_i\right) = 0 \tag{1}$$

$$\frac{\partial}{\partial t}\left(\rho u_i\right) + \frac{\partial}{\partial x_j}\left(\rho u_i u_j\right) = \frac{\partial}{\partial x_j}\left(-\, p\delta_{ij} + \sigma_{ij}\right) \tag{2}$$

$$\frac{\partial}{\partial t}\left(\rho h\right) + \frac{\partial}{\partial x_j}\left(\rho u_j h\right) = \frac{\partial p}{\partial t} + \frac{\partial}{\partial x_j}\left(\frac{\mu}{\mathrm{Pr}}\frac{\partial h}{\partial x_j}\right) \tag{3}$$

where ρ, u_i, p are the density, velocity, pressure and the mixture enthalpy per unit mass, respectively.

δ_{ij} is the Kronecker delta function, μ represents the molecular viscosity and Pr is Prandtl number. The viscous stress tensor σ_{ij} is defined as:

$$\sigma_{ij} = \mu\left[\frac{\partial u_i}{\partial x_j} + \frac{\partial u_j}{\partial x_i} - \frac{2}{3}\left(\frac{\partial u_k}{\partial x_k}\right)\delta_{ij}\right] \tag{4}$$

The system is completed by the equation of state:

$$p = \rho R_{gaz} T \tag{5}$$

where R_{gaz} is the gas constant and T represents the temperature.

Lighthill idea was to express the fundamental equations of motion into a wave equation for acoustic fluctuation with a source term on the right-hand side. Subtracting the space derivative of the momentum equation, Eqn. (1) one obtains:

$$\frac{\partial^2 \rho}{\partial t^2} - \frac{\partial^2}{\partial x_i \partial x_j}\left(\rho u_i u_j\right) = \frac{\partial^2}{\partial x_i \partial x_j}\left(p\delta_{ij} - \sigma_{ij}\right) \tag{6}$$

This expression is equivalent

$$\frac{\partial^2 \rho}{\partial t^2} - \frac{\partial^2}{\partial x_i \partial x_j}\left(\rho u_i u_j\right) = \frac{\partial^2}{\partial x_i \partial x_j}\left(p\delta_{ij} - \sigma_{ij}\right) + c_0^2 \frac{\partial^2 \rho}{\partial x_i^2} - \frac{\partial^2}{\partial x_i \partial x_j}\left(c_0^2 \rho \delta_{ij}\right) \tag{7}$$

where c_0 denotes the speed of sound in the uniform medium. Equation (7) can be rearranged in order to obtain a wave equation on the left-hand side and the acoustic sources on the right-hand side:

$$\frac{\partial^2 \rho}{\partial t^2} - c_0^2 \frac{\partial^2 \rho}{\partial x_i^2} = \frac{\partial^2}{\partial x_i \partial x_j}\left(\rho u_i u_j\right) + \frac{\partial^2}{\partial x_i \partial x_j}\left[\left(p - c_0^2 \rho\right)\delta_{ij}\right] - \frac{\partial^2}{\partial x_i \partial x_j}\left(\sigma_{ij}\right) \tag{8}$$

The acoustic source due to the viscosity effects can be neglected since it can be proved that is proportional with the inverse of the Reynolds number. Accordingly, the contribution of the viscous stresses to the total acoustic source term is therefore unimportant. Lighthill's wave equation for the density becomes:

$$\frac{\partial^2 \rho}{\partial t^2} - c_0^2 \frac{\partial^2 \rho}{\partial x_i^2} = \frac{\partial^2}{\partial x_i \partial x_j}\left(\rho u_i u_j\right) + \frac{\partial^2}{\partial x_i \partial x_j}\left[\left(p - c_0^2 \rho\right)\delta_{ij}\right] \tag{9}$$

A decomposition of the flow variables can be introduced:

$$u_i = u_{0i} + u_i' \qquad p = p_0 + p' \qquad \rho = \rho_0 + \rho' \tag{10}$$

where u_i', p', ρ' are defined as small perturbations (acoustic fluctuations) from a state where the fluid is at rest with a uniform density ρ_0 and a uniform pressure p_0; one can obtain Lighthill acoustic analogy, formulated in terms of acoustic density fluctuation (ρ'):

$$\frac{\partial^2 \rho'}{\partial t^2} - c_0^2 \frac{\partial^2 \rho'}{\partial x_i^2} = \frac{\partial^2 T_{ij}}{\partial x_i \partial x_j} \tag{11}$$

Equation (11) describes a distributed source of sound, where the acoustic source term can be seen as negligible outside the flow where only generated sound waves are present. The inhomogeneity in Eqn.(11) is given by the "forcing term" (total acoustic source term) on the right-hand side, which is responsible for generation of sound and is a second order spatial derivative of the Lighthill stress tensor T_{ij}:

$$T_{ij} = \rho u_i u_j + \left[\left(p - p_0\right) - c_0^2\left(\rho - \rho_0\right)\right]\delta_{ij} \tag{12}$$

The acoustic source is due to the flow field gradients and due to the compressibility effects.

Thus, the total acoustic source term (T_{total}) can be decomposed into velocity variations related acoustic (T_I) and entropy effects related acoustic (T_{II}) source terms, respectively:

$$\frac{\partial^2 T_{ij}}{\partial x_i \partial x_j} = \frac{\partial^2 \left(\rho u_i u_j\right)}{\partial x_i \partial x_j} + \frac{\partial^2 \left[\left(p - c_0^2 \rho\right)\delta_{ij}\right]}{\partial x_i \partial x_j} \tag{13}$$

$$T_I = \frac{\partial^2 \left(\rho u_i u_j\right)}{\partial x_i \partial x_j};\ T_{II} = \frac{\partial^2 \left[\left(p - c_0^2 \rho\right)\delta_{ij}\right]}{\partial x_i \partial x_j}$$

3. NUMERICAL METHODS

In this section, the numerical methods are presented for the Lighthill's analogy. A solution procedure can have several steps. First, a computational grid that depends upon the geometrical configuration of the flow field is introduced. For the spatial discretization of the governing equations, a Cartesian stagnation grid is used.

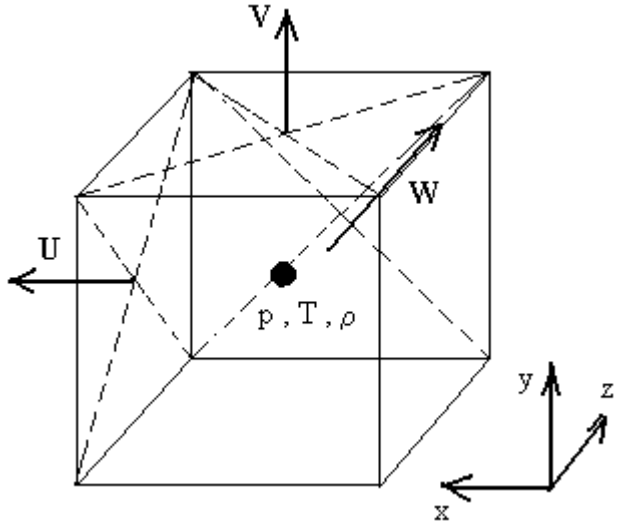

Fig.2. Computational cell in a three dimensional staggered grid

Staggered grid means that the variables are stored at different locations in each computational cell. The velocity components are stored at the cell faces, while the pressure, temperature and density are stored in the cell center, fig. 2.

The governing equations are discretized on the grid. This means that the differential equations are converted into a system of algebraic equations that can be solved numerically. For the discretization of Eqs. (11), the following relations are used:

$$\left(\frac{\partial^2 \rho'}{\partial x_i^2}\right)_{k,l} = \frac{\rho'_{k+1,l} - 2\rho'_{k,l} + \rho'_{k-1,l}}{\left(\Delta x_i\right)^2} + O\left(\Delta x_i^2\right), \qquad i = 1,2,3$$

$$\left(\frac{\partial^2 \rho}{\partial x_i \partial x_j}\right) = \frac{\rho'_{k+1,l+1} - \rho'_{k+1,l-1}}{4\Delta x_i \Delta x_j} - \frac{\rho'_{k-1,l+1} - \rho'_{k+1,l-1}}{4\Delta x_i \Delta x_j} + O(\Delta x_k^2, \Delta x_l^2)$$

$$\left(\frac{\partial^2\rho'}{\partial t^2}\right)_n = \frac{\rho'^{n+1}_{k+l} - 2\rho'^{n}_{k,l} + \rho'^{n-1}_{k,l}}{(\Delta t)^2} + O(\Delta t^2)$$

$$\frac{\partial^2 T_{ij}}{\partial x_k \partial x_l} = \sigma_{k,l}$$

The Lighthill wave equation has the discretized form:

$$a_1\rho'_{k+1,l} + a_2\rho'_{k,l} + a_3\rho'_{k-1,l} + b_1\rho'_{k,l+1} + b_2\rho'_{k,l} + b_3\rho'_{k,l-1} = \sigma_{k,l}$$

where:

$$a_1 = \frac{1}{(\Delta t)^2} + \frac{1}{(\Delta x_i)^2} + \frac{1}{4\Delta x_i \Delta x_j}$$

$$a_2 = -\frac{2}{(\Delta t^2)} - \frac{1}{2(\Delta x_i^2)} - \frac{2}{\Delta x_i \Delta y_j}$$

$$a_3 = \frac{1}{(\Delta t)^2} + \frac{1}{(\Delta x_i)^2} + \frac{1}{4\Delta x_i \Delta x_j}$$

$$b_1 = \frac{1}{\Delta t^2} + \frac{1}{(\Delta x_j)^2} + \frac{1}{4\Delta x_i \Delta x_j}$$

$$b_2 = \frac{-2}{\Delta t^2} + \frac{1}{(\Delta x_j)^2} + \frac{1}{4\Delta x_i \Delta x_j}$$

$$b_3 = \frac{1}{\Delta t^2} + \frac{1}{(\Delta x_j)^2} + \frac{1}{4\Delta x_i \Delta x_j}$$

The discretized equation is solved in the cell [-3,3]x[-3,3]x[-3,3], where the spatial steps are $\Delta x_i = 0.001$ and time step, $\Delta t = 0.01$. For the function $\sigma_{k,l}$, constant values in the plane (x,y,0) are considered so that they represent the function's image depending on ρ' and the curves $\rho' = const.$, the wave front.

The wall boundary condition requires a zero value of the ρ'.

4. RESULTS AND CONCLUSIONS

Solving the Lighthill's wave equation one can obtain the numerical simulation of noise source generation and research the phenomenon propagation and wave interference of acoustic waves over the surface of aerodynamic profile.

The first example is the numerical simulation for the generation of acoustic source monopole located in surface centre (0,0). In fig. 3 the distribution of radiant intensity of

source (fluid density over aerodynamic surface) can be observed and fig. 4 shows the constant density curves (wave front). The concentricity of wave front can be observed, because the environment of propagation is homogeneous and isotropic. Near the boundary of the aerodynamic profile, the wave front is similar to profile. This fact denotes the strong influence of boundary conditions that are considered for solving the equations. Possibly, the wave interference phenomenon can be noticed in the profile corner, where practically there is no acoustics wave. The next example is the numerical generation of monopole acoustic source placed at the edge of profile, in the stagnation point (-3,0).

In fig. 5 are presented the constant density curves for this case.

Fig. 6 presents the distribution of constant density curves for two monopole sources placed as follows: the first in the stagnation point and the second in the detachment point. The symmetry of curves distribution around the two noise sources can be noticed.

If a point obstacle placed in detachment point over the profile surface (3.0) is examined the interference between incident wave and reflected wave by the total reflection conditions can be observed.

Fig. 7 shows the 3D the image of the radiant intensity of distribution of two sources and in fig. 8 are represented the constant density curves**.** It is possible to observe that the level of intensity is low because through the interference of two waves, which are in phase opposition, his resultant minimizes or is zero.

To highlight the results of the previous experiment, let's consider the interference between the incident wave and two reflected wave on two obstacles placed in corners of an aerodynamic surface, in coordinated points,(3,-3) and (3,3).

In fig. 9 are represented in 3D the radiant intensities distribution of the three sources, and in fig. 10 are represented the level constant density curves.

As in the previous experiment it was found that the level of this curves is very low, and the zero zones of profile surface prevail.

In the previous cases, the numerical results are for the extreme time moments, when the equations solutions and the flow are stabilized, and monopole source generated waves with fundamental frequency. When the equations are numerically solved for a monopole source that generates a higher frequency (the source with many tonal) and for short time moments (before the stabilization of equations solutions), the results are represented in fig. 11 and 12.

REFERENCES

[1] Mihai Mihaescu, *Computational Aero acoustics Based on Large Eddy Simulation and Acoustic Analogies,* Thesis for the degree of Doctor of Philosophy in Engineering, Lund, Sweden, April, 2005.

[2] H. Dumitrescu, V. Cardos, F. Frunzulica, A. Dumitrache, *Aerodinamica nestationara, Aeroelasticitate si Aeroacustica pentru turbine de vant,* Editura Academiei Romane, 2007.

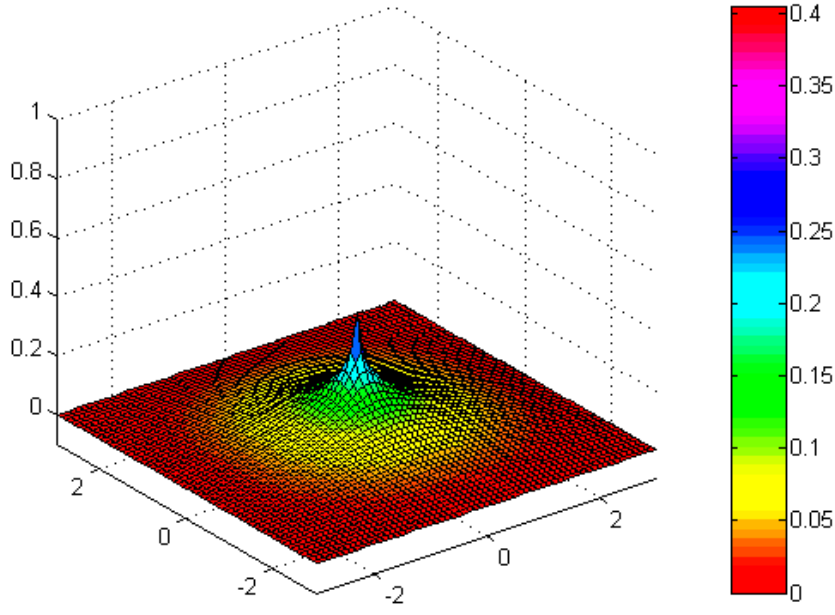

Fig.3. The 3D image of monopol source

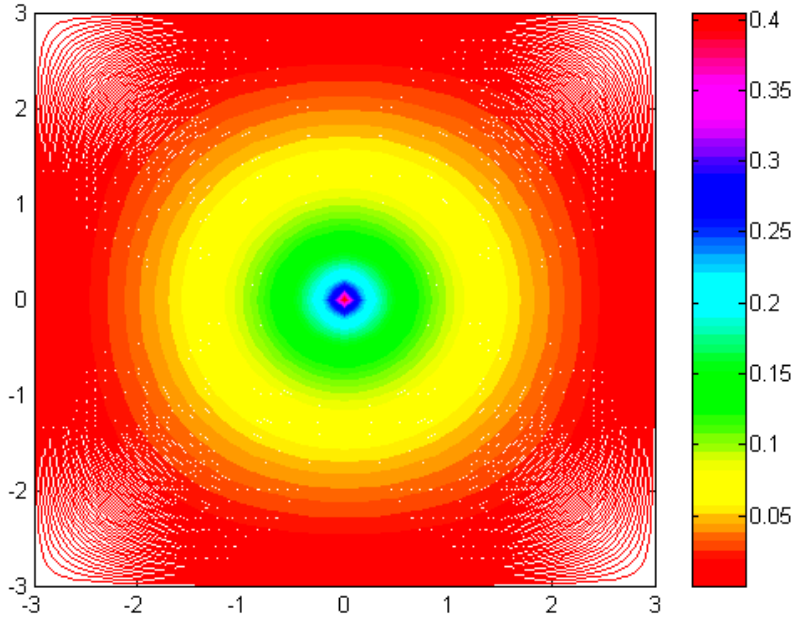

Fig. 4. The density's constant curves

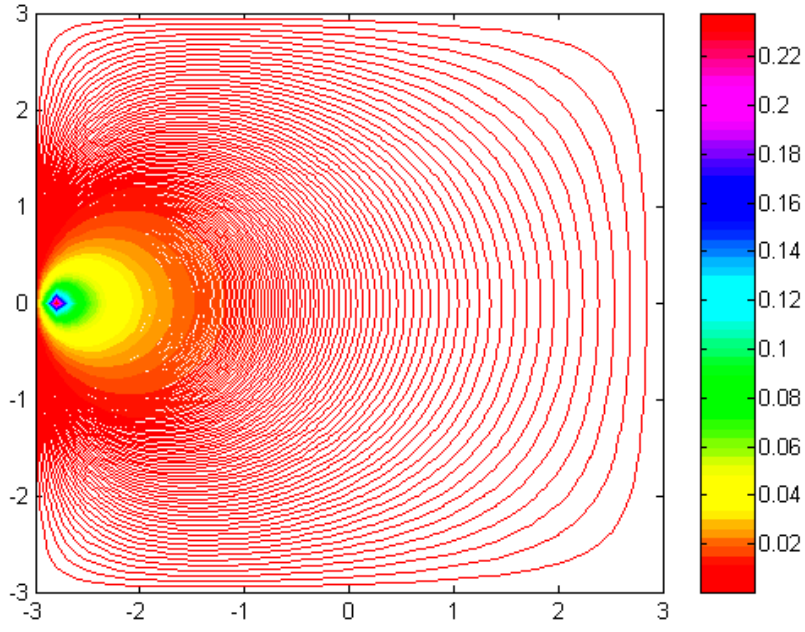

Fig.5. The density's constant curves

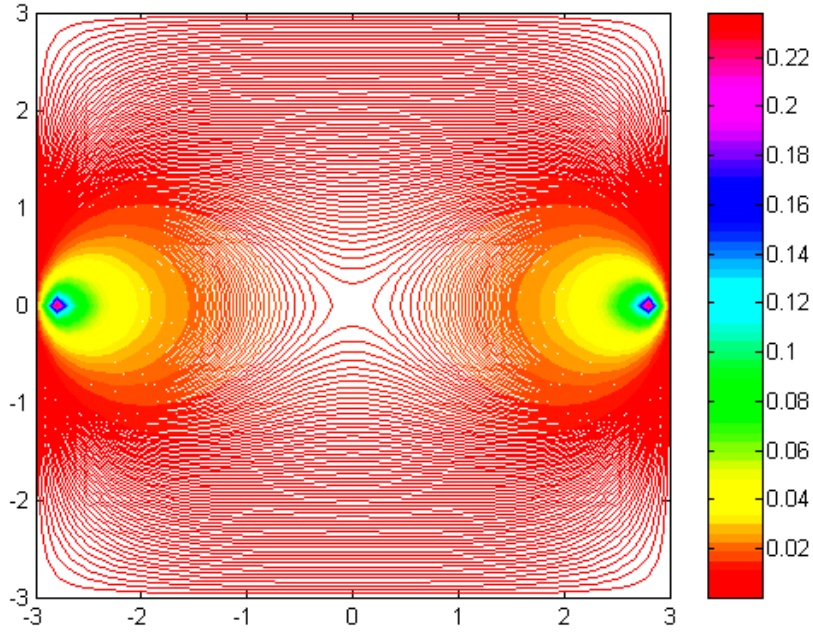

Fig.6 The density's constant curves

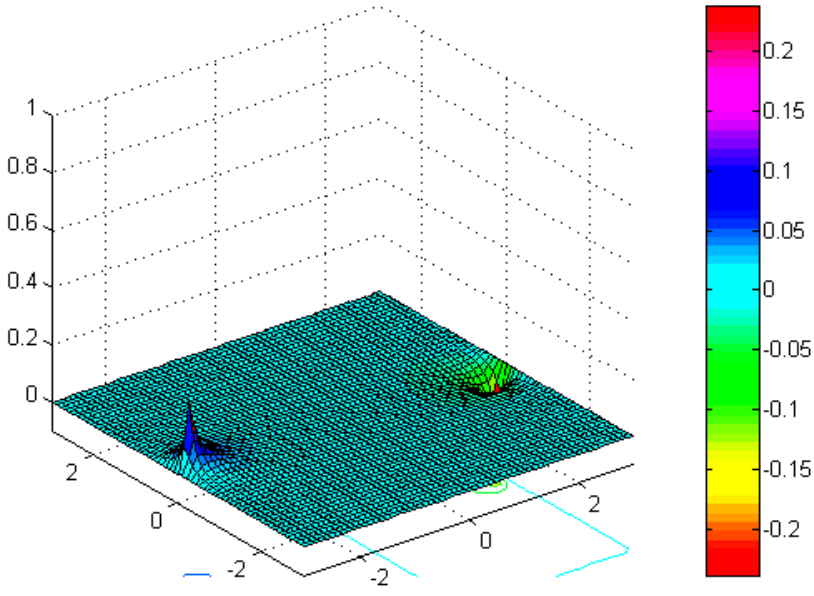

Fig.7. The 3D image of monopol source

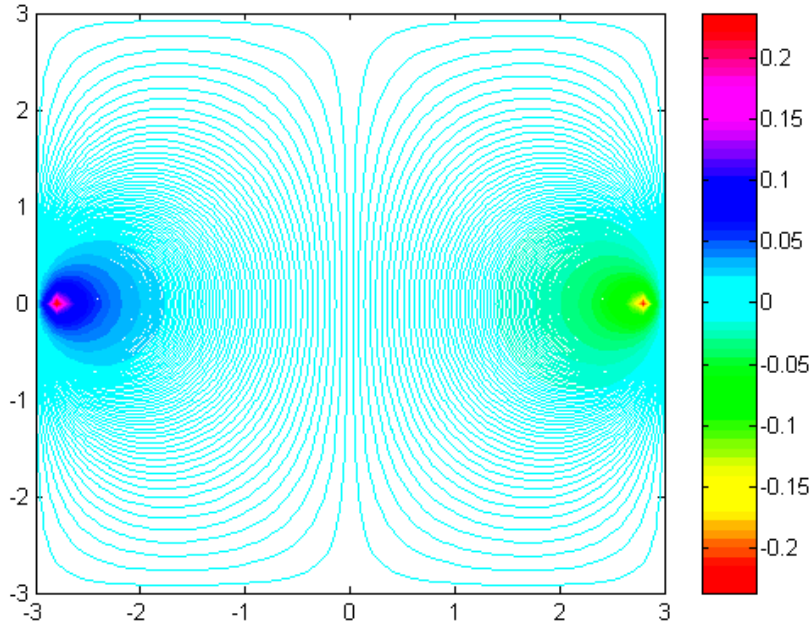

Fig.8. The density's constant curves

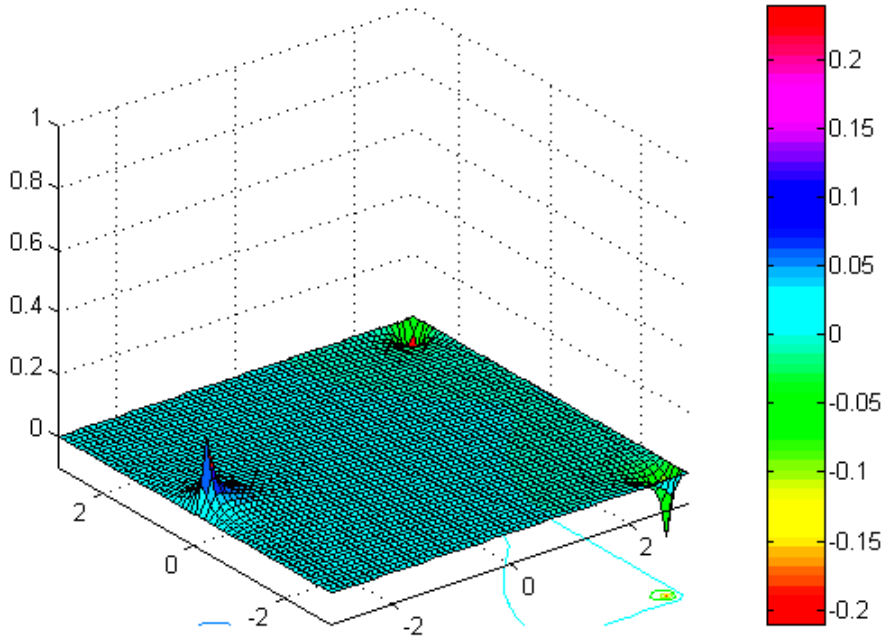

Fig.9 The 3D image of monopol source

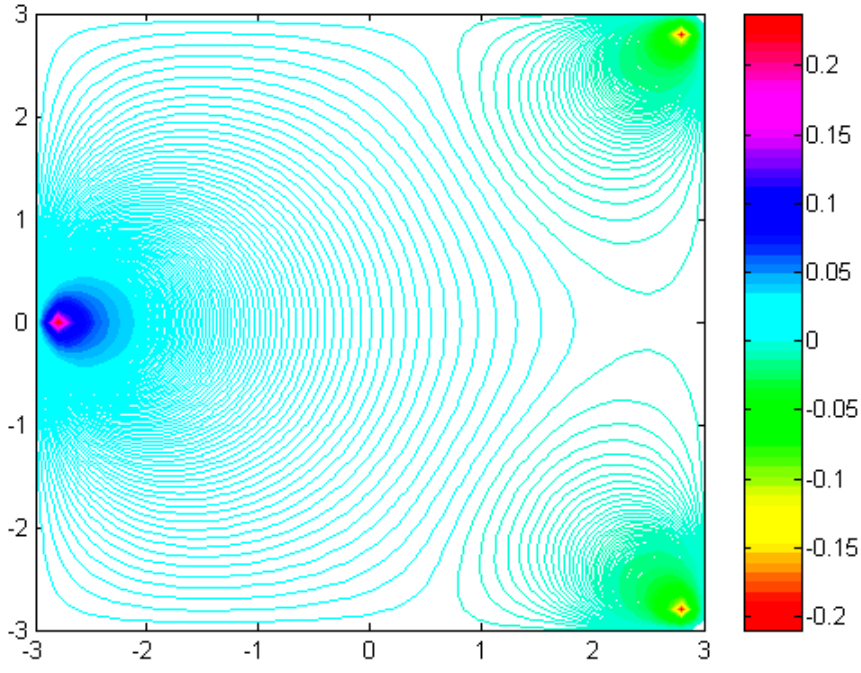

Fig.10. The density's constant curves

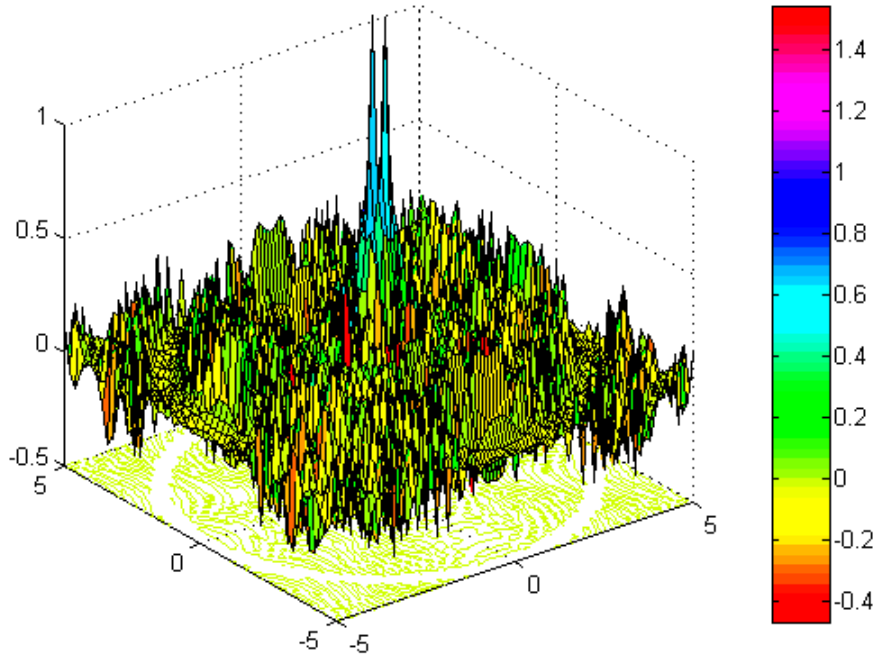

Fig.11 The 3D image of monopol source

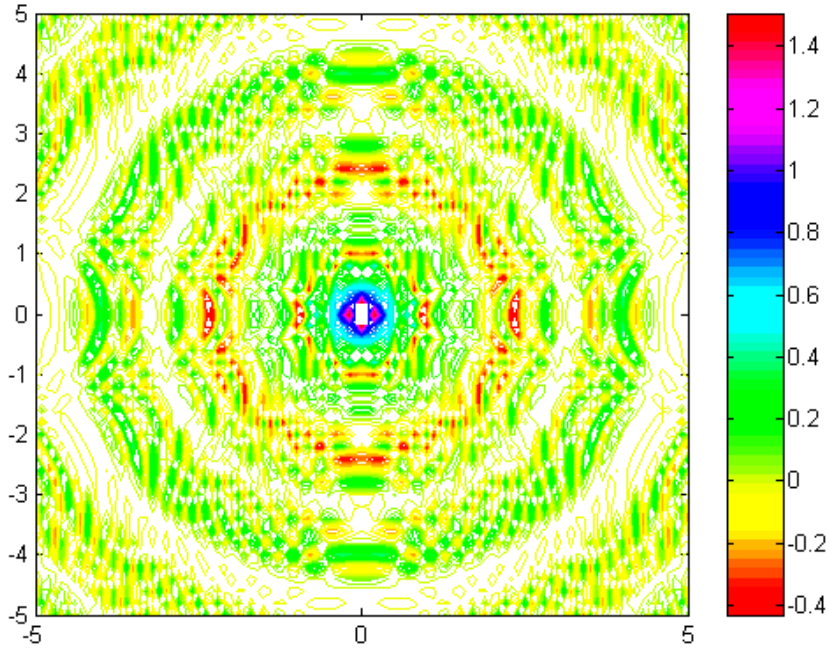

Fig.12. The density's constant curves